Analysis of an integrated heating and cooling system for a building complex with focus on long-term thermal storage

Daniel Rohde[a],*, Trond Andresen[b], Natasa Nord[a]

[a] Norwegian University of Science and Technology. Kolbjørn Hejes vei 1A, 7491 Trondheim, Norway

[b] SINTEF Energy Research. Sem Sælands vei 11, 7034 Trondheim, Norway

* Corresponding author. E-mail address: daniel.rohde@ntnu.no

Abstract

Modern building complexes have simultaneous heating and cooling demands. Therefore, integrated energy systems with heat pumps and long-term thermal storage are a promising solution. An integrated heating and cooling system for a building complex in Oslo, Norway was analyzed in this study. The main components of the system were heat pumps, solar thermal collectors, storage tanks, ice thermal energy storage, and borehole thermal energy storage. Dynamic simulation models were developed in Modelica with focus on the long-term thermal energy storage. One year measurement data was used to calibrate the system model and two COPs were defined to evaluate system performance. The simulation results showed that more heat had to be extracted from the long-term thermal storage during winter than could be injected during summer. This imbalance led to a decrease in ground temperature (3 °C after 5 years) and decreasing long-term performance of the system: both COPs decreased by 10 % within five years. This performance decrease could be avoided by increasing the number of solar collectors from 140 to 830 or by importing more heat from the local district heating system. Both measures led to sustainable operation with a balanced long-term thermal storage.

Keywords: Modelica, Heating and cooling system, Heat pumps, Borehole thermal energy storage

Nomenclature

Abbreviations

BTES   Borehole thermal energy storage
COP   Coefficient of performance
DH   District heating
DHW   Domestic hot water
GSHP   Ground source heat pump
HP   Heat pump
HX   Heat exchanger
ITES   Ice thermal energy storage

1

IHCS   Integrated heating and cooling system

NTU   Number of transfer units

Symbols

a_1 Linear heat loss coefficient [W/(m^2·K)]

a_2 Quadratic heat loss coefficient [W/(m^2·K^2)]

η   Efficiency (-)

ΔT   Temperature difference (K)

A   Area (m^2)

C   Heat capacity rate (W/K)

c_p Specific heat capacity [J/(kg·K)]

ε   Heat exchanger effectiveness (-)

El   Electricity use (kWh)

FtP   Flow-to-power coefficient (W·s^2/m^6)

$\dot{m}$ Mass flow rate (kg/s)

Nu   Nusselt Number (-)

P   Power (W)

q   Exponent for calculation of heat transfer coefficient (-)

$\dot{Q}$ Heat flow rate (W)

R   Solar radiation per m^2 (W/m^2)

T   Temperature (K)

U   Heat transfer coefficient [W/(m^2·K)]

V   Volume (m^3)

$\dot{V}$ Volume flow rate (m^3/s)

Subscripts

amb   Ambient

cold   Cold side

col   Solar collector

cond   Condenser

const   Constant

evap   Evaporator

hot   Hot side

HP   Heat pump

in   Inlet

L   Lorentz

max   Maximum

meas   Measured

min   Minimum

nom   Nominal

2

opt	Optical
out	Outlet
pumps	Circulation pumps
r	Ratio
sec	Secondary

1   Introduction

Buildings account for a large share of the world's energy use, with a share of around 40 % in the European Union [1]. Nearly 55 % of this energy is used for space heating, domestic hot water (DHW) heating, and space cooling [2]. Many efforts have been made to reduce the carbon emissions related to these thermal energy demands. Emissions can be reduced by decreasing the demands themselves, e.g. through better building envelopes and/or advanced control strategies, or by delivering the thermal energy at lower carbon costs, e.g. using more efficient energy systems and/or renewable energy sources.

District heating and cooling systems cover the heating and cooling demands of many buildings. The efficiency of such systems depends mainly on their energy sources and distribution losses. Much research is focused on 4th generation district heating (DH) and smart thermal grids [3]. On a smaller scale, micro-grids or integrated heating and cooling systems can be a promising solution, especially for new areas or major retrofitting projects [4, 5]. Ground source heat pumps (GSHP) are an efficient technology to cover both heating and cooling demands, especially when they are combined with thermal energy storage [6]. Thermal storage is most effective when short and long-term storage are combined [7]. However, the annual heat balance of the long-term storage is an important aspect. For borehole thermal energy storages, the average temperature of the ground changes if the amounts of extracted and rejected heat differ. This ground temperature change will lead to reduced system efficiency after long-term operation as reported in [8-12]. GSHP systems for heating-dominated buildings are therefore often combined with solar thermal collectors to charge the long-term storage during summer to avoid a ground temperature decrease [13-15].

The inherent dynamics of thermal storage require dynamic simulation models for analysis. TRNSYS is a well-known commercial tool for dynamic simulations, which has been used for similar analyses in [16-19]. A common alternative is the open, object-oriented language Modelica, which has also been applied successfully for system analyses with thermal storage, see [20-23]. Modelica was chosen for this study because its high level of flexibility enables the development of specialized and fast simulation models.

A coefficient of performance (COP) is often used to evaluate system performance. However, many different COPs can be defined which makes it difficult to compare absolute values from different

systems. Published COP values for system performance from systems similar to the one in this study were 3.3 (in heating period) [13], up to 3.4 [24], 3.8 [8], and 3.3 to 4.2 [17].

An integrated heating and cooling system (IHCS) for a small neighborhood in Oslo, Norway was described and analyzed in this study. Dynamic simulations were performed to analyze the system performance of the IHCS and all models were developed with the aim of a good trade-off between accuracy and simulation time. Focus was on the annual heat balance of the long-term thermal storage and its influence on the system performance. A new COP including this heat balance was defined.

This paper is structured as follows: the system description can be found in Section 2. In Section 3, the simulation models, the system control, and the sensitivity analysis are explained. Results from the simulations are presented in Section 4, followed by a discussion in Section 5 and concluding remarks in Section 6.

2 System description

2.1 The integrated heating and cooling system

An area of about 100 x 200 m in the Norwegian capital Oslo was renewed with several buildings and an integrated heating and cooling system (IHCS). Construction was completed in 2014 and the IHCS supplied a total floor area of 38500 m^2. The supplied building types and their respective floor areas are shown in Table 1.

Table 1. Building floor area supplied by the IHCS.

Type	Offices	Shops	Hotels	Apartments	Food court	Event location	Total
Floor area (m^2)	15000	6650	7600	3900	3500	1850	38500

The IHCS delivered thermal energy for space heating, DHW heating, snow melting, space cooling, and product cooling. Snow melting was applied to the walkways between the buildings and product cooling was only delivered to the food court. A schematic of the IHCS is shown in Figure 1.
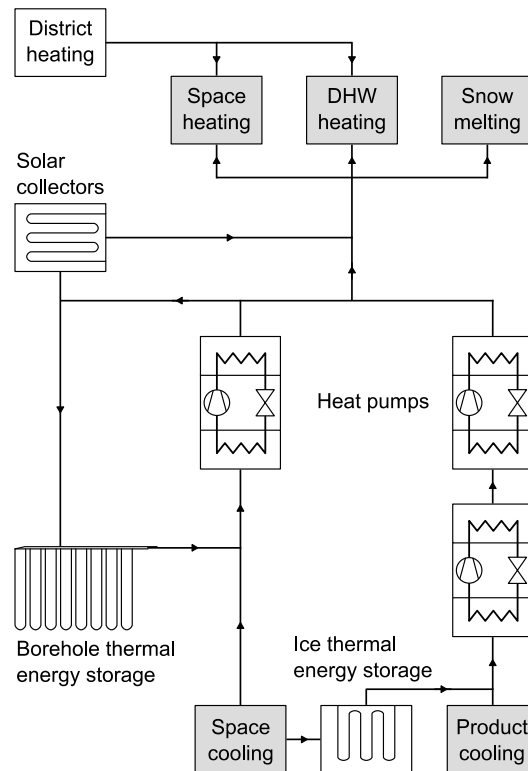
4

Figure 1. Simplified overview of the integrated heating and cooling system.

The main components of the IHCS shown in Figure 1 were heat pumps, heat exchangers, solar collectors, storage tanks, ice thermal energy storage (ITES), and borehole thermal energy storage (BTES). During heating season, the BTES and the surplus heat from space cooling and product cooling were used as heat sources on the evaporator side of the heat pumps. The condenser heat from the heat pumps was sent to space heating, DHW preheating, and snow melting. During cooling season, a lot of surplus heat was available from the cooling systems, which needed to be released on the condenser side of the heat pumps. In addition, the solar collectors also delivered heat and only a part of this heat was needed for space heating and DHW preheating. Therefore, heat was injected into the BTES during cooling season. The ITES was used to reduce space cooling peak demands during summer. The ITES was charged during the night and discharged during the day.

The IHCS was designed to deliver heat at 50-55°C and was also connected to the city's DH system, which delivered heat at a temperature of 85-120°C. This DH connection was used as backup (in case of system failure), for peak demand coverage, and as temperature lift for DHW heating, which had a supply temperature setpoint of 70°C. A more detailed description of the IHCS including heat pump specifications can be found in [25].

Table 2: Heat pump specifications

	HP 1	HP 2	HP 3	HP 4 & 5
Type	WSA2802X	WSA1602X	WSA0701X	NXW0600X
Working fluid	R134a	R134a	R134a	R410a
Compressor	Screw (2)	Screw (2)	Screw	Scroll
Design data cooling (evap/cond)				
Temperatures	4.5°C / 48°C	4.5°C / 48°C	20°C / 55°C	-8°C / 25°C
Capacities	595 / 772 kW	334 / 436 kW	224 / 283 kW	87 / 110 kW
COP	4.36	4.27	4.80	4.78
Design data heating (evap/cond)				
Temperatures	0°C / 50°C	0°C / 50°C		
Capacities	473 / 652 kW	264 / 365 kW		
COP	3.64	3.61		

2.2   Measurement data

The IHCS was equipped with a control and monitoring platform. Energy meters were installed to measure the delivered energy for heating and cooling in each connected building. However, no energy meters were installed to measure the energy exchange with the BTES or the performance of the solar collectors. Only the total electricity use of the system was measured, so the electricity use of single components was also not available. The amount of DH import was measured for each building.

Data from the building energy management system for the year 2015 was used in this study. The total heating demand was 3562 MWh and the total cooling demand was 1585 MWh. The values for each demand type as well as measured electricity use and DH import are shown in Figure 2.
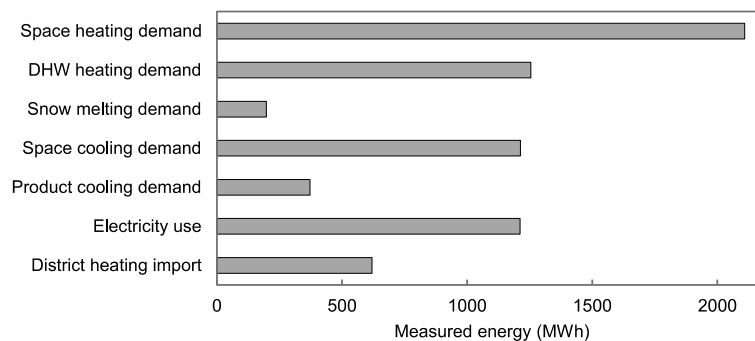

Figure 2. Measured energy amounts for 2015.

The on-site temperature was only measured by one sensor and solar radiation was not measured at all. Therefore, ambient temperature and solar radiation data from nearby weather stations were retrieved [26]. The on-site temperature was found to be around 5°C higher than nearby measurements, which might be due to the location of the sensor or an offset error. Therefore, 5°C were subtracted from the measured on-site temperature for the simulation input file. The input file also contained data for

6

solar radiation from the nearest weather station. Other weather data like rain- and snowfall or wind speed were excluded from the analysis.

3   Methodology

The modelling approach that was chosen for this study is explained in this chapter. After some general information, the key component models are explained in detail, followed by a description of the system model and the system control. Afterwards, the sensitivity analysis is described.

The simulation models were developed using the open, object-oriented language Modelica [27]. Dymola was used as simulation environment and the standard solver DASSL was chosen with a tolerance of $1e^{-5}$. All models were developed with the aim to run parameter studies that require many model evaluations. Thus, low simulation time was an important requirement for the system model and a good trade-off between accuracy and simulation time was sought.

The library «Thermal», which is included in the «Modelica Standard Library» [28], was used as basis for the developed component models. However, many elements from the library were modified to increase simulation speed. All fluids were assumed incompressible and all fluid properties were assumed constant. The required fluid properties were calculated in Excel using the add-in CoolProp [29].

3.1   Component models

3.1.1   Heat exchanger model

All heat exchangers in the IHCS were counterflow plate heat exchangers. The heat flow rate from hot to cold fluid ($\dot{Q}$) was calculated with the effectiveness-NTU method [30]. The implemented relation for the effectiveness (ε) of a counterflow heat exchanger is shown in Equations 1 to 6. Measures were taken to avoid numerical instabilities at zero flow conditions and at $C_r = 1$, which both led to division by zero in some of the equations. The total heat transfer area (A) as well as nominal conditions for mass flow rate ($\dot{m}_{nom}$) and overall heat transfer coefficient (U_{nom}) were input parameters of the model.

$$C = \dot{m} \cdot c_p \tag{1}$$

$$C_{min/max} = min/max(C_{hot}, C_{cold}) \tag{2}$$

$$C_r = \frac{C_{min}}{C_{max}} \tag{3}$$

$$NTU = \frac{U \cdot A}{C_{min}} \tag{4}$$

$$\varepsilon = \frac{1 - exp[-NTU \cdot (1 - C_r)]}{1 - C_r \cdot exp[-NTU \cdot (1 - C_r)]} \tag{5}$$

7

$$\dot{Q} = \varepsilon \cdot C_{min} \cdot \left(T_{hot\_in} - T_{cold\_in} \right) \tag{6}$$

The overall heat transfer coefficient (U) in Equation 4 was continuously calculated based on nominal and actual flow conditions according to [31], see Equation 7.

$$U = U_{nom} \cdot \frac{\left(\dot{m}_{hot\_nom} \right)^{-q} + \left(\dot{m}_{cold\_nom} \right)^{-q}}{\left(\dot{m}_{hot} \right)^{-q} + \left(\dot{m}_{cold} \right)^{-q}} \tag{7}$$

Equation 7 assumes similar heat transfer on both sides of the heat exchanger and negligible conduction resistance of the heat exchanger plates. The exponent q defines the influence of changes in mass flow rate on the heat transfer coefficient and lies in the order of 0.7 according to [31]. The Nusselt number for typical brazed plate heat exchanger configurations increases with $Re^{0.63}$ according to [32]. Therefore, q was set to 0.63.

3.1.2 Heat pump model

A heat pump consists of a closed thermodynamic cycle including two heat exchangers. These function as condenser and evaporator of the cycle's working fluid on the primary side. The heat sink and the heat source are connected to the condenser and the evaporator on the secondary side, respectively. The heat pump model used for this study was based on the theoretical Lorentz cycle. It is similar to the well-known Carnot cycle, but does not assume the heat source and sink to be isothermal. Instead, they have a finite heat capacity and thus change temperature during heat addition/extraction [33], which is the case for the fluid flows of the IHCS. Therefore, the Lorentz COP (COP_L) depended on both inlet and outlet temperatures on the secondary sides and required the calculation of the Lorentz temperature (T_L) for condenser and evaporator as shown in Equations 8 and 9. The COP_L was multiplied with a constant Lorentz efficiency (η_L) to calculate the heat pump's COP (COP_{HP}), see Equation 10.

$$T_{L\_cond/evap} = \frac{T_{in\_sec\_cond/evap} - T_{out\_sec\_cond/evap}}{\ln \left(\frac{T_{in\_sec\_cond/evap}}{T_{out\_sec\_cond/evap}} \right)} \tag{8}$$

$$COP_L = \frac{T_{L\_evap}}{T_{L\_cond} - T_{L\_evap}} \tag{9}$$

$$COP_{HP} = COP_L \cdot \eta_L \tag{10}$$

$$\dot{Q}_{cond/evap} = \dot{m}_{sec\_cond/evap} \cdot c_p \cdot \left(T_{in\_sec\_cond/evap} - T_{out\_sec\_cond/evap} \right) \tag{11}$$

$$P_{HP} \cdot COP_{HP} = \dot{Q}_{evap} \tag{12}$$

$$P_{HP} + \dot{Q}_{evap} = \dot{Q}_{cond} \tag{13}$$

The Lorentz efficiency was an input parameter of the model and was chosen based on manufacturer specifications. The specifications included design data for different operating conditions, which allowed the calculation of η_L for each operating condition. Operating conditions that were not

8

relevant were excluded and the average of the relevant values for η_L was used in this study. Values from 0.384 to 0.461 were obtained. This conforms well with the work of Østergaard and Andersen, where the Lorentz efficiency was also used as input parameter with values of 0.4 for small heat pumps and 0.5 for large heat pumps [34].

The mass flow rates ($\dot{m}_{sec\_cond/evap}$) and inlet temperatures ($T_{in\_sec\_cond/evap}$) on the secondary sides were calculated in the system model. One of the outlet temperatures on the secondary sides ($T_{out\_sec\_cond/evap}$) had to be set by an input signal to the heat pump model. The other outlet temperature and the required heat pump power (P_{HP}) could then be calculated. This approach was much faster and more stable than using P_{HP} as input signal and calculating both outlet temperatures in the model.

3.1.3 Borehole thermal energy storage model

A cross section model of the BTES was developed and several of these cross sections were connected in series to model the BTES. The three main parts of a BTES were included in the cross section model: a single U-tube pipe, the borehole with filling material, and the surrounding ground. A schematic and the simulation model are shown in Figure 3.
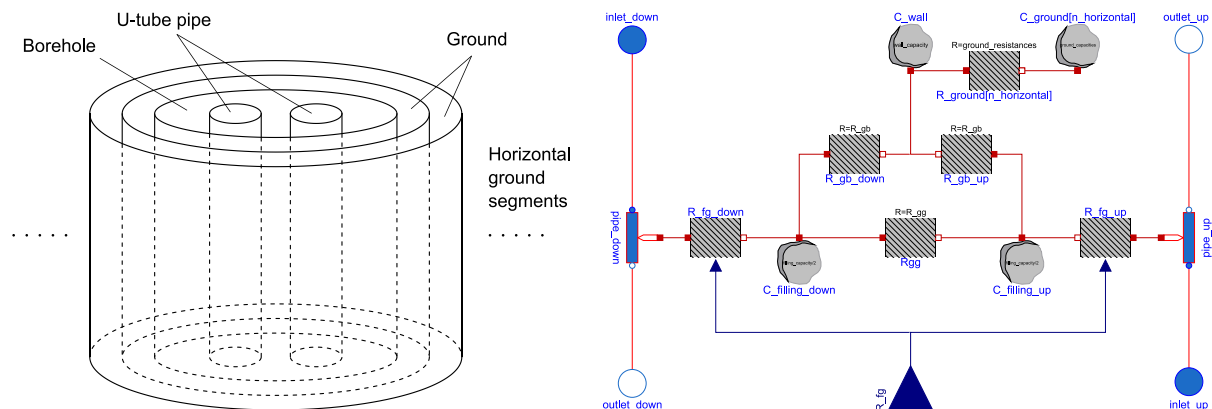

Figure 3. BTES cross section model (left: schematic, right: simulation model).

The U-tube pipe segments in each cross section were modeled as fluid with uniform temperature. The borehole filling and the surrounding ground were modeled as thermal capacities. Thermal resistances were added to model two-dimensional heat transfer between the fluid in the pipe and the borehole wall according to the methodology published by Bauer et al. [35]. The thermal resistances were calculated based on equations 16-21, 31, 33, and 42 in [35]. The thermal resistance between fluid and filling material depended on the fluid mass flow rate due to the convective resistance inside the pipe. As fluid properties were assumed constant, Equation 14 was used to approximate the Nusselt number for the convective term of the thermal resistance. The equation was based on the Nusselt correlation for turbulent pipe flow. Nu_{nom} was set to 160 and $\dot{m}_{nom}$ was set to 0.8 kg/s.

9

$$Nu = Nu_{nom} \cdot \left(\frac{\dot{m}}{\dot{m}_{nom}} \right)^{0.8} \tag{14}$$

The boreholes of the IHCS were filled with groundwater. Natural convection inside groundwater-filled boreholes may have a significant influence on the performance of the ground heat exchanger [36]. Nusselt correlations for this natural convection were published by Spitler et al. [37] and Holmberg et al. [38]. Holmberg et al. investigated a ground heat exchanger similar to the ones of the IHCS and found the Nusselt number to be 6.4 during heat injection and 3.68 during heat extraction. A constant Nusselt number of 5.0 was used for the system simulations.

One-dimensional, radial, heat transfer was modeled in the cylindrical ground shells. The capacities and heat transfer coefficients corresponded to the geometry of each shell element according to [39]. The conductivity of the ground at the location of the IHCS is about 2.75 with a standard deviation of 0.65 according to Ramstad et al. [40]. The pipe segments were connected from each cross section to the next, but no thermal connection was modeled between the thermal capacities of the cross sections. Nevertheless, the horizontal discretization of the ground was found to be more important than the vertical discretization. Therefore, the horizontal discretization was set to 30 and the vertical discretization was set to 4 as shown in Table 3.

Table 3. BTES model specifications used for system simulations.

Parameter	Value	Unit	Parameter	Value	Unit
Borehole depth	300	m	Number of boreholes	62	-
Borehole diameter	0.14	m	Vertical discretization	4	-
Ground diameter	9	m	Horizontal discretization	30	-
Ground density	2600	kg/m^3	U-tube diameter	0.04	m
Ground heat capacity	850	J/(kg·K)	U-tube conductivity	0.42	W/(m·K)
Ground conductivity	2.75	W/(m·K)	Nusselt number inside borehole	5	-

The initial temperature of the ground had to be defined in the model. However, the temperature distribution was unknown, since the IHCS had been in operation before 2015. It was assumed that there was heat left to be extracted from previous charging of the BTES. A linear profile in radial direction was assumed for the initial temperature, ranging from 25°C for borehole and pipe to 10°C for the outmost ground capacity.

Arranging boreholes in a pattern and connecting them in series can increase the performance of a BTES, as described for example in [41]. The boreholes of the IHCS were drilled in a rectangular pattern with a rather large distance of eight meters and were connected in parallel. In the model, cylindrical shells were used and a diameter of nine meters was chosen to give a similar effective ground area between the boreholes. The assumed homogeneity of the ground led to identical temperatures for the outmost ground shell of all boreholes. Thus, no heat was transferred between boreholes in the model.

10

The BTES was used as seasonal thermal energy storage. However, the short-term response of the ground heat exchangers can also play an important role for system performance [42-44]. Beier et al. published experimental data for a 52-hour charging period of a grouted single U-tube borehole heat exchanger surrounded by wet sand [45]. The short-term response of the BTES model developed in this study was validated against this experimental data set. The experimental setup was imitated by changing the model specifications in Table 3 to the respective values of the experimental setup and using the measured inlet temperature and mass flow rate as simulation input. The simulated outlet temperature, the average wall temperature, and three average ground temperatures at different distances from the borehole were compared to the measured values from [45]. The developed model showed very good agreement with the measurement data as shown in Figure 4.
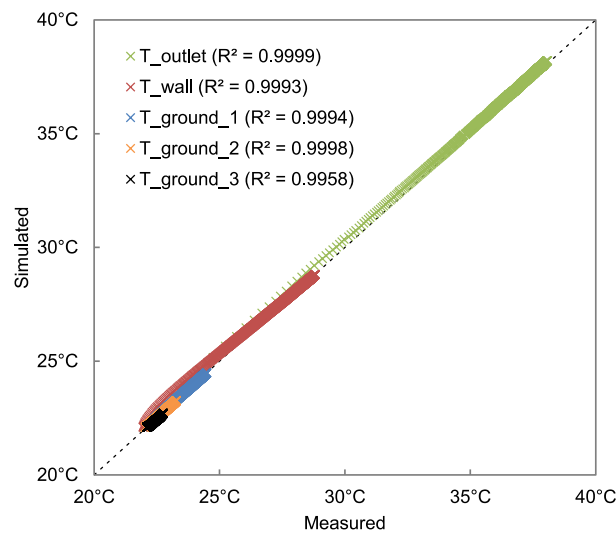

Figure 4. BTES model validation against experimental data from [45].

3.1.4 Solar collector model

The installed collectors were flat plate solar collectors. The net heat flow rate for each collector ($\dot{Q}_{col}$) was calculated with Equation 15, based on the widely used European Standard EN 12975-1:2006.

$$\dot{Q}_{col} = A_{col} \cdot \left[R \cdot \eta_{opt} - a_1 \cdot (T_{col} - T_{amb}) - a_2 \cdot (T_{col} - T_{amb})^2 \right] \tag{15}$$

The solar radiation (R) was an input signal to the model and T_{col} was the average fluid temperature in the collector. For each installed collector, the effective area (A_{col}) was 1.9 m^2, the optical efficiency (η_{opt}) was 0.773, and the linear and quadratic heat loss coefficients (a_1 and a_2, respectively) were 3.676 W/(m^2·K) and 0.0143 W/(m^2·K^2). The fluid filling in each collector was 1.2 liters.

Collectors in series were modeled individually with respective flow connections. The interaction of parallel collectors was neglected and distributing headers were not modeled. Herrero López et al. compared a simple collector model with a more detailed model and measurement data. They concluded that a simple model, like the one developed for this study, is well suited for system analysis [46].

11

3.1.5 Storage tank model

Storage tanks were modeled by dividing the fluid in the tanks into several horizontal layers. These layers were assumed to have a uniform temperature and the flow inside the tank was one-dimensional with the inlet and outlet of the tanks at the tank top and bottom (multi-node model as explained by Dumont et al. [47]). Internal heat exchange between the layers and heat transfer to the ambient were neglected.

The storage tank model for the solar collector loop was extended with an internal counterflow heat exchanger. The fluid in the heat exchanger was divided into the same number of layers as the storage tank with the same assumptions of uniform temperature and one-dimensional flow. The heat exchanger fluid was thermally connected to the tank fluid with a constant conductivity in each layer. The conductivity value was scaled based on the total effective area of the solar collectors. 100 W/K per m^2 of collector area was found to be a reasonable value. The volume of the solar storage tank and its internal heat exchanger were also scaled with a value of 15 and 1.5 dm^3 per m^2 of collector area, respectively.

3.1.6 Substation model

A substation model was developed, which represented the connection of the IHCS to the buildings. A heat exchanger transferred heat between the fluid loop of the IHCS and the building side. A fixed return temperature on the building side was assumed and pumps on each side were controlled to achieve the required heat flow rate. The heat flow rate was an input signal to the model. In the system model, these signals were based on the measured heating and cooling demands.

The IHCS was not designed to cover all heating demands. DH was used to cover peak demands for space heating and to lift the temperature of the DHW to the desired level. The amount of DH import was calculated based on the remaining heating demand.

The IHCS had separate heat exchangers for each building and demand type, which were connected to the heating and cooling loops in parallel. These parallel heat exchangers were modeled as one heat exchanger with the same total area and average heat transfer coefficient.

3.1.7 Ice thermal energy storage model

The ITES had a capacity of around 400 kWh. A nightly charging profile was created based on the nominal cooling capacity of the charging heat pump. Charging started at midnight with a constant cooling rate of 87 kW until the 400 kWh were reached. This charging profile was used as input signal for a substation model, which was connected to the low temperature loop of the IHCS and thus represented the charging of the ITES. A discharging profile with a maximum of 100 kW cooling rate was also created. The 400 kWh were distributed over seven hours (25 kW, 50 kW, 75 kW, 100 kW, 75 kW, 50 kW, and 25 kW) and the peak discharge hour was matched with the maximum space cooling

12

demand each day. This profile was then deducted from the space cooling demand signal during cooling mode to represent the discharging of the ITES.

3.2   System model

The system model consisted of connected component models and a control system. All components and fluids were specified as close as possible to manufacturer specifications. Hourly values for all heating and cooling demands as well as ambient temperature and solar radiation were input data for the system model. Spline interpolation was used to create continuous signals between the hourly data points. The required CPU time for a one-year simulation was around 70 seconds with an Intel® Core™ i7-6700K (4GHz) and 64 GB RAM. The model is shown in Figure 5.
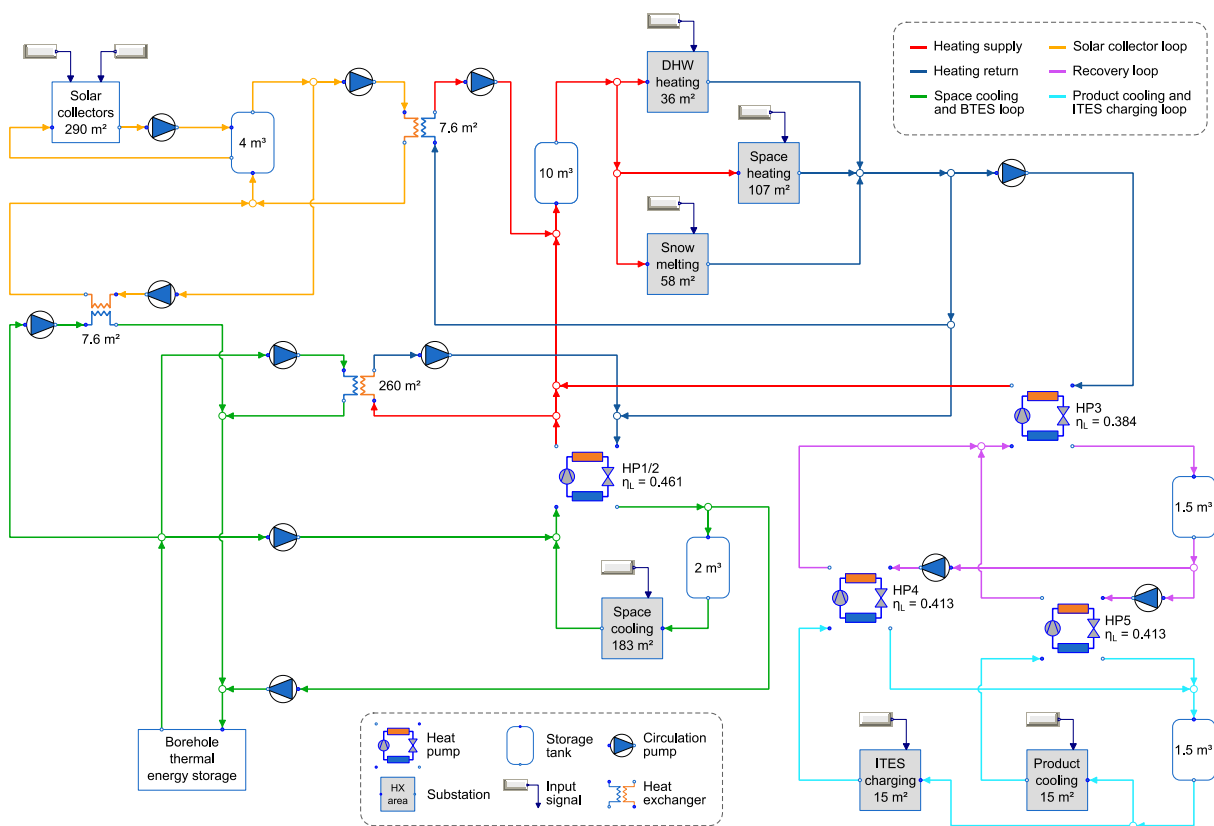

Figure 5. System model with selected specifications.

HP1/2 in Figure 5 represented two parallel heat pumps of the same type. These were modeled as one unit because their efficiencies were very similar. Pipes connecting the components of the IHCS were not modeled because specifications were not available. Distribution heat losses from the IHCS were thus not calculated. However, the losses from the distribution systems of the buildings were included in the measured demands.

The calculated electricity use of the system consisted of three parts: the electricity use of the heat pumps (El_{HPs}), the electricity use of the circulation pumps (El_{pumps}), and a constant term (El_{const}).

13

El_{HPs} was calculated by integrating the simulated power of each heat pump (P_{HP}). The circulation pump models did not calculate pump power because pressure drops could not be calculated realistically due to missing pipe specifications. The relatively constant electricity use of all auxiliary systems was also unknown. Therefore, a system-level approach was chosen to calculate El_{pumps} and El_{const}. El_{pumps} was assumed proportional to the squared volume flow rate ($\dot{V}$) of the circulation pumps and was multiplied with a constant flow-to-power coefficient (FtP). FtP and El_{const} were found by calibrating the monthly calculated electricity use to the measured values with Equation 16.

$$\min \sum_{i=1}^{12} \left[El_{meas} - \left(El_{HPs} + \underbrace{FtP \cdot \sum \dot{V}_{pumps}^2}_{El_{pumps}} + El_{const} \right) \right]^2 , \; i = \text{month of the year} \qquad (16)$$

Equation 16 gave a value of $70.65e^6$ for FtP and a constant electricity use of 30.5 kW. The monthly values for electricity use after the calibration are shown in Figure 6.
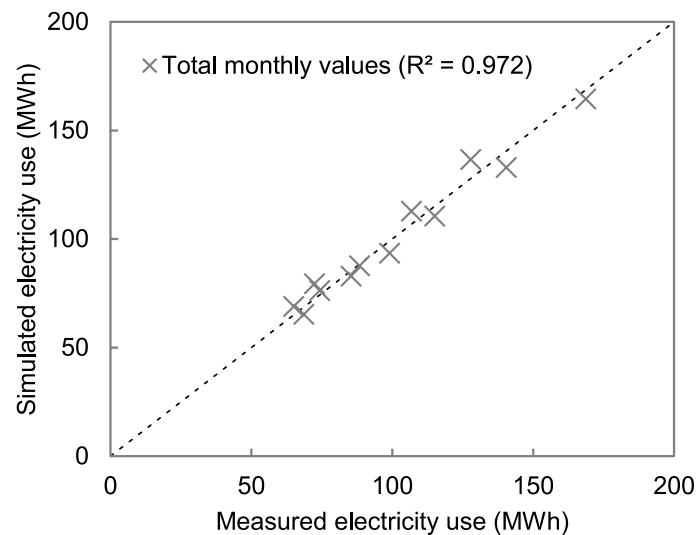

Figure 6. Calibration of electricity use in system model.

3.3 System control

The IHCS was equipped with a simple control system. The heat pumps received stepwise control signals to activate/deactivate their parallel circuits and compressor stages. These step signals were based on storage tank temperatures. The circulation pumps were controlled based on pressure difference setpoints or temperature setpoints. The storage tanks were only used as buffers.

In the system model, the heat pumps were controlled continuously since the individual compressor stages were not included in the heat pump model. The circulation pumps were controlled with PI-controllers based on temperature setpoints. The PI-controller outputs were limited to avoid unrealistically high mass flow rates.

14

The two operation modes of the IHCS, heating mode and cooling mode, are explained in the sections below. The real system required some downtime for a mode switch due to manual valve adjustments. Therefore, only one mode switch was performed between heating and cooling season. In the system model, this downtime was neglected and several mode switches were allowed. Models from the library «StateGraph», which is included in the «Modelica Standard Library» [28], were used to switch between modes based on the storage tank temperatures. A mode switch involved the activation/deactivation of the BTES circulation pumps, a change in heating supply temperature setpoint, and different control strategies for the solar collectors and the ITES.

3.3.1 Heating mode

In heating mode, the outlet temperature of HP1/2 on the condenser side was set to equal the heating supply temperature of 55°C. The outlet temperature on the evaporator side of HP1/2 was controlled by the BTES pump with the space cooling supply temperature of 6°C as setpoint. Rule-based control was applied for the solar collector loop. The solar storage tank could be used for heating supply and BTES charging. Heating supply was prioritized with a floating collector outlet temperature 10°C above solar storage tank top temperature, similar to [48]. If the temperature in the solar storage tank was too low for heating supply, the BTES was charged. The ITES was not used in heating mode.

When the space cooling demand increased, less heat had to be extracted from the BTES. At some point, the BTES was not needed as heat source and the temperature in the cooling storage tank increased. When the average temperature in the cooling storage tank was higher than 10°C, a mode switch was triggered to ensure that the space cooling demand could be covered.

3.3.2 Cooling mode

In cooling mode, the outlet temperature of HP1/2 on the evaporator side was set to equal the space cooling supply temperature of 6°C. The outlet temperature on the condenser side of HP1/2 was controlled by the BTES pump with a reduced heating supply temperature of 51°C as setpoint. The solar collectors were only used for BTES charging in cooling mode. The ITES was used to reduce space cooling peak demands and was charged by HP4 during the night.

When the heating demands increased, less heat was available to be injected into the BTES. At some point, the BTES was not needed as heat sink and the temperature in the heating storage tank decreased due to the increasing heat demands. When the average temperature in the heating storage tank was lower than 47°C, a mode switch was triggered to ensure that the heating demands could be covered.

3.4 System performance and sensitivity analysis

Two COPs were defined to measure system performance: COP_{system} and $COP_{system+storage}$. These were evaluated at the end of each one-year simulation. COP_{system} was the ratio of the heating and cooling

15

energy delivered by the IHCS to the electricity used by the IHCS as shown in Equation 17. The amount of imported heat from the DH system was not included.

$$COP_{system} = \frac{\text{Heating delivered} + \text{Cooling delivered}}{\text{Electricity used}} \tag{17}$$

$COP_{system+storage}$ was similar to COP_{system} but included the annual heat balance of the BTES (heat injected – heat extracted) in the numerator as shown in Equation 18. The heat balance was included because it affected long-term operation. $COP_{system+storage}$ thus gave a more holistic indication of system performance by penalizing unsustainable operation.

$$COP_{system+storage} = \frac{\text{Heating delivered} + \text{Cooling delivered} + \text{Heat balance BTES}}{\text{Electricity used}} \tag{18}$$

A sensitivity analysis was performed to evaluate the influence of selected input parameters on the system performance. Parameters were changed one at a time and the difference in COP compared to the base case scenario was calculated. A 20 % change was chosen as standard value. However, some parameters were varied by a different percentage as shown in Table 4. The values for heating and cooling supply temperature were chosen to give a 20 % change in the temperature difference in the heat exchanger of the space heating and space cooling substations. The values for the return temperatures in the substations were also chosen to change this temperature difference by 20 %.

16

Table 4. Parameter values used for sensitivity analysis.

Parameter	Unit	Lower value	Base case	Upper value	Change	Comment
Numerical discretization						
Factor storage tanks	-	0.8	1.0	1.2	20 %	
Factor BTES	-	0.8	1.0	1.2	20 %	
Uncertain inputs						
BTES: Nusselt number	-	3.5	5.0	6.5	30 %	According to [38]
BTES: Initial temp. (near)	°C	22	25	28	12 %	3°C chosen instead of
BTES: Initial temp. (far)	°C	7	10	13	30 %	percentage
BTES: Ground conductivity	W/(m·K)	2.10	2.75	3.40	24 %	According to [40]
η_L HP1/2	-	0.410	0.461	0.512	11 %	According to
η_L HP3	-	0.346	0.384	0.422	10 %	manufacturer specifications (all HPs
η_L HP4&5	-	0.339	0.413	0.487	18 %	changed at once)
Exponent q in HX	-	0.504	0.630	0.756	20 %	Equation 7
Coefficient FtP	-	$56.52e^6$	$70.65e^6$	$84.78e^6$	20 %	Equation 16
Assumptions						
Space heating return temp.	°C	37	40	43	8 %	
Snow melting return temp.	°C	13	20	27	35 %	Secondary side changed
Space cooling return temp.	°C	13.2	15.0	16.8	12 %	to give 20 % change in ΔT
Product cooling return temp.	°C	-5.2	-4.0	-2.8	30 %	
Heating/cooling demands						
Demand factor all	-	0.8	1.0	1.2	20 %	All demands multiplied
Demand factor heating	-	0.8	1.0	1.2	20 %	Only heating demands
Demand factor cooling	-	0.8	1.0	1.2	20 %	Only cooling demands
Control setpoints						
Mode switch ΔT	°C	3.2	4.0	4.8	20 %	Heating/cooling mode
Heating supply temp.	°C	52	55	58	5 %	Primary side changed to
Space cooling supply temp.	°C	4.2	6.0	7.8	30 %	give 20 % change in ΔT
System design						
Factor HX area	-	0.8	1.0	1.2	20 %	All areas multiplied
Number of solar collectors	-	110	140	170	21 %	
Number of boreholes	-	50	62	74	19 %	

The number of solar collectors was changed during the sensitivity analysis. The number of serial collectors was set to five and the number of parallel collectors was changed. The storage tank with internal heat exchanger was scaled based on the total collector area as explained in Section 3.1.5. The area of the heat exchangers in the solar collector loop were also scaled to avoid bottlenecks. The maximum mass flow rate of the BTES pump was linearly scaled when the number of boreholes was changed.

4   Results

The results from the system analysis are described in this chapter. First, the base case scenario results are analyzed and compared to the measurement data. Afterwards, the results from the sensitivity analysis are presented and solutions to avoid performance degradation are suggested.

4.1   Base case scenario

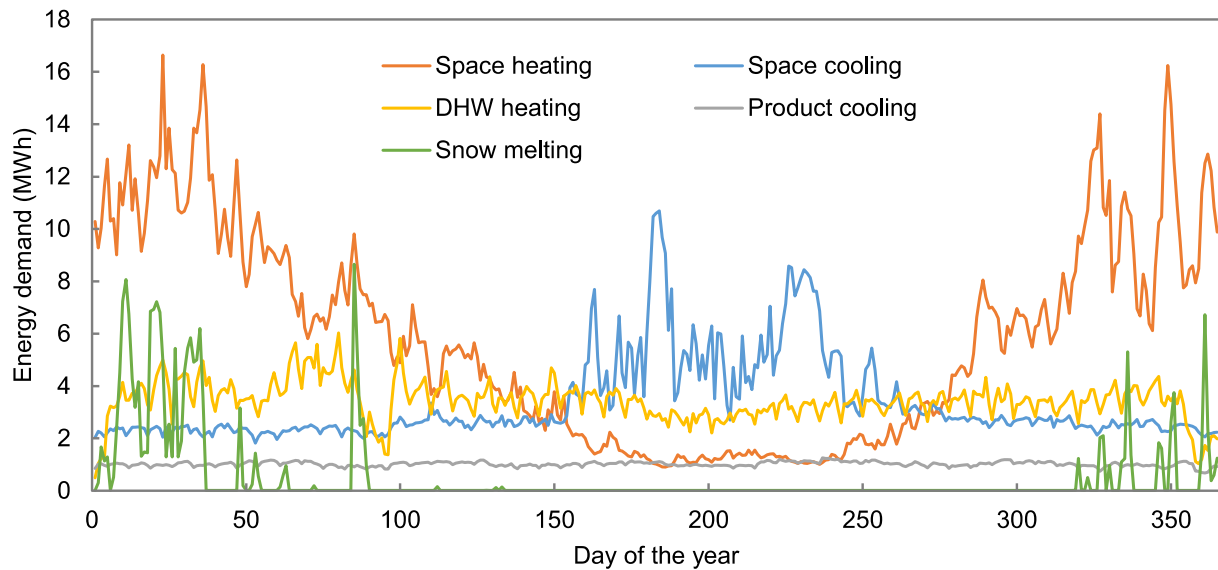Daily values for the measured heating and cooling demands are shown in Figure 7.

Figure 7. Measured daily heating and cooling demands.

Space heating and cooling showed typical seasonal variations, while the DHW heating and product cooling depended on the users. Snow melting depended on temperature and precipitation and thus showed large daily variations. These demands were covered by the IHCS. Daily amounts of electricity and DH import used for this are shown in Figure 8.
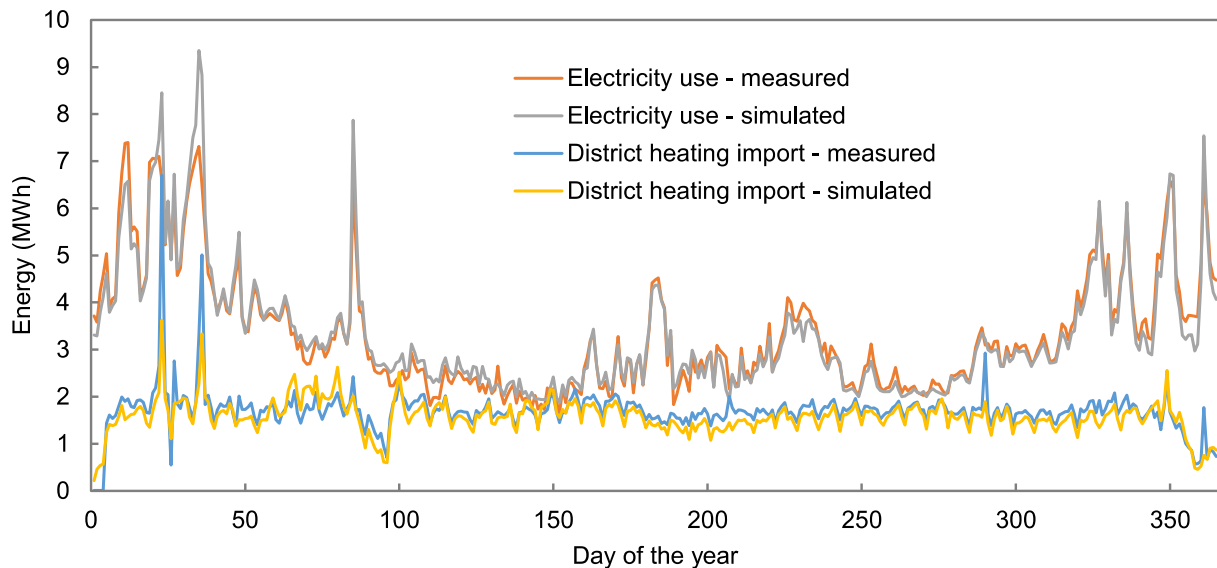
18

Figure 8. Daily energy use of the integrated heating and cooling system.

It can be seen from Figure 7 and Figure 8 that higher demands led to higher energy use. The main source of electricity use were the heat pumps, which had a share of 69 % for the base case scenario. To recall, the electricity use of single components was not measured, so no reference value for this simulation result was available. The simulated daily values for electricity use and DH import showed good agreement with the measured values as shown in Figure 8. However, large differences occurred at the beginning of the year during peak heating demands. For the real system, these peak demands led to high amounts of DH import (blue line) because the heat pumps were only able to cover a small share of these demands. In the simulated system, the heat pumps covered a larger share, which led to less simulated DH import (yellow line), but more electricity use (gray line vs. orange line). The heat pump models did not exceed the maximum power listed in the manufacturer specifications, so the overestimation of electricity use was most likely due to the calculated pumping power. The BTES pumps accounted for 58 % of the total pumping power for the base case scenario simulations, so a more detailed model of the BTES loop might improve these results.

Integral annual energy use values and R^2-values for hourly and daily results are shown in Table 5 for all the demands, DH import, and electricity use.

Table 5. Comparison of measured and simulated values.

	Measured MWh	Simulated MWh	Difference MWh	R² hourly -	R² daily -
Space heating from IHCS	2096	2104	8	0.993	0.998
Space heating from DH	13	5	-8	0.454	0.812
Space cooling from IHCS	1213	1211	-2	0.928	0.997
DHW heating from IHCS	648	682	35	0.867	0.897
DHW heating from DH	607	572	-35	0.629	0.723
Product cooling from IHCS	372	372	0	0.972	1.000
Snow melting from IHCS	198	198	0	0.998	1.000
Electricity use IHCS	1212	1212	0	0.849	0.942

As explained in Section 2.2, measurements for the BTES and the solar collectors were unfortunately not available. The simulated daily heat balances for both components are shown in Figure 9.
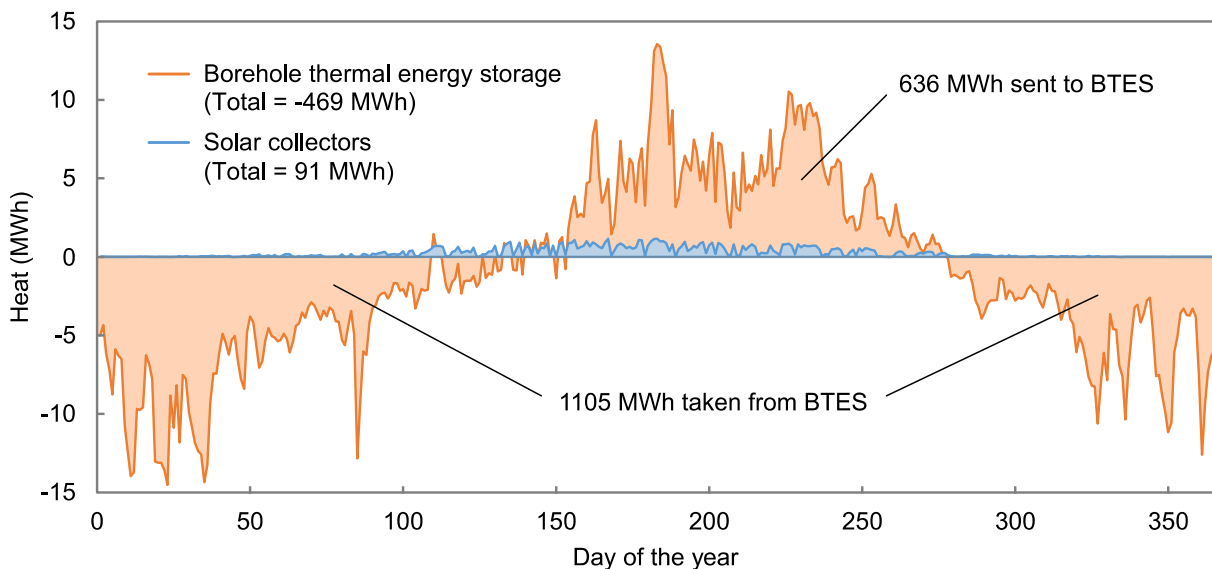

Figure 9. Simulated daily heat balance for BTES and solar collectors.

Figure 9 clearly shows that the BTES was used as heat source during winter and as heat sink during summer, with a simulated annual heat balance of -469 MWh. The maximum heat flow rates were -856 kW during winter and 946 kW during summer. This corresponded to specific heat flow rates of -46 and 51 W/m of borehole, respectively. This is reasonable according to [49], where 50 to 80 W/m are listed as expected peak values.

The simulated amount of collected solar heat was 91 MWh, see Figure 9. This corresponded to 2.6 % of the total heating demands, which showed that the solar collectors played a minor role for the performance of the IHCS.

20

Monthly values for COP_{system} ranged from 3.3 to 4.2 for the base case scenario, with an annual average of 3.77. The annual average for $COP_{system+storage}$ was 3.38. These values were similar to the ones from other studies described in the introduction.

4.2 Sensitivity analysis

The results from the sensitivity analysis showed the relative change of each COP when a parameter value was increased or decreased, see Figure 10.
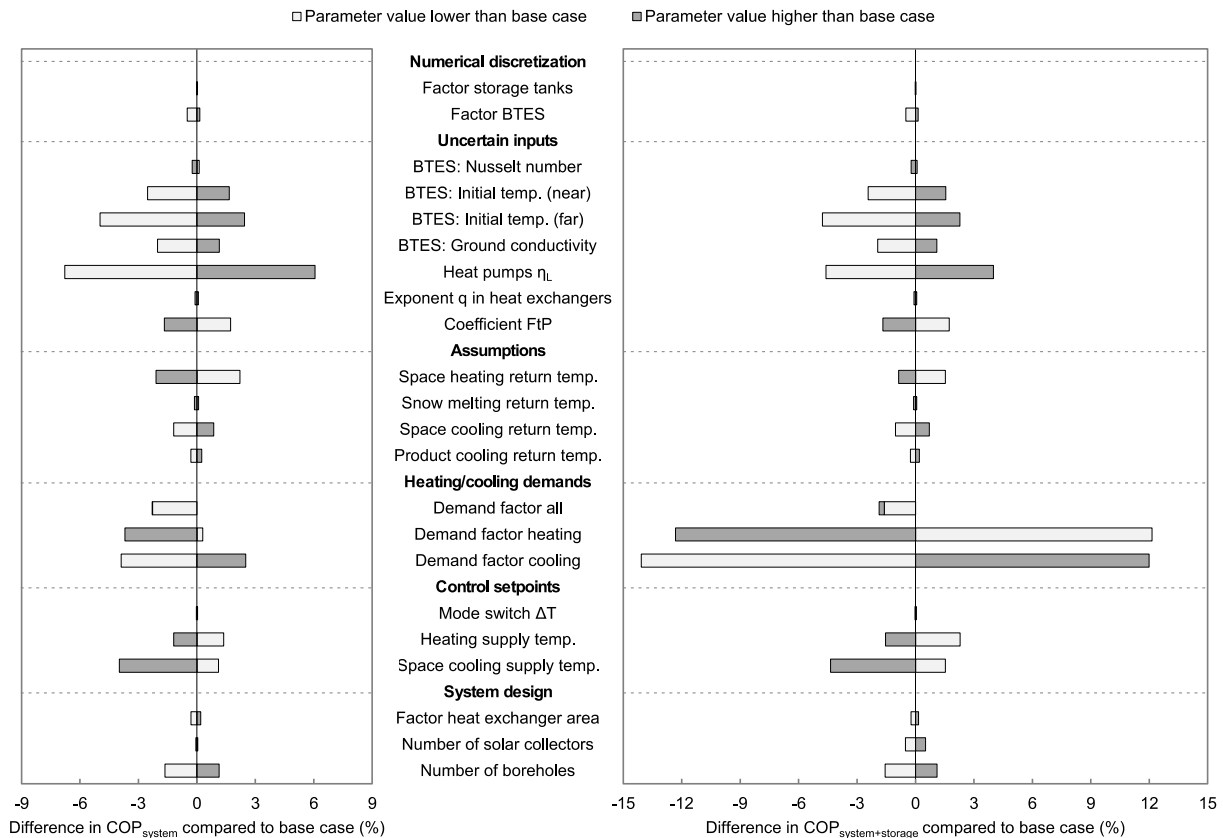

Figure 10. Sensitivity analysis results.

The most important results from the sensitivity analysis are described below.

Increasing the numerical discretization had a negligible effect on the COPs. A reduction in discretization of the BTES led to a decrease of 0.5 %, which shows that the base case scenario values were reasonable.

Some of the uncertain inputs influenced the COPs significantly. The heat pumps were the main electricity users, which is why their efficiency had a strong influence, especially on COP_{system}, see Figure 10 (left). The initial temperature profile and the conductivity of the ground also showed strong influence on the COPs, while the Nusselt number for natural convection inside the borehole and the heat exchanger exponent q used in Equation 7 were less important.

21

The return temperatures from the buildings' heating and cooling systems were assumed constant in this study. The influence of the assumed temperatures depended on the total amount of delivered energy, which is why the main demand (space heating) had the strongest influence on the COPs. In reality, the return temperatures can show larger variations than in this sensitivity study. Therefore, a more realistic calculation of the return temperatures could show larger influence on the system performance and should be included in future work. This is especially desirable for the space heating substation where the largest amount of heat was transferred.

The heating and cooling demands were based on the available measurements. The cooling demands were heat sources for the IHCS and the heating demands were heat sinks. Therefore, the difference between the total heating demand and the total cooling demand highly influenced the annual heat balance of the BTES. Changing all demands simultaneously thus altered the BTES balance less than changing only heating or cooling demands. This is why changing all demands showed less effect than changing only heating or cooling demands, especially for $COP_{system+storage}$.

The control setpoint for a mode switch had insignificant influence on the system performance due to the small number of mode switches during a year. The supply temperature setpoints changed the heat pump outlet temperatures and thus affected both the temperature lift of the heat pumps and the mass flow rates of the circulation pumps. Especially an increase in space cooling supply temperature showed strong influence on the COPs.

The system design parameters showed little effect on the COPs. Only a change in the number of boreholes changed the COPs by more than 1 %. This change in COP was mainly due to the difference in required pumping power. The BTES outlet temperature changed slightly when the number of boreholes was changed, which in turn led to a small change in the heat pump's COP. However, the annual heat balance of the BTES did not change significantly, since almost the same amounts of energy had to be injected/extracted each day.

4.3   Long-term operation analysis and system performance degradation

The simulated annual heat balance of the BTES was -469 MWh for the base case scenario due to the high heating demands and the insufficient solar charging, see Figure 9. Two solutions to avoid a negative heat balance were analyzed in this study: the installation of more solar collectors and the increase of DH import for DHW heating.

4.3.1   Case I: More solar collectors

For this case, the number of solar collectors was increased until the annual heat balance of the BTES was close to zero. To achieve this balanced BTES, the number of collectors had to be increased from 140 to 830. This increased the simulated amount of collected solar heat from 91 MWh, as shown

22

in Figure 9, to 565 MWh. There is free roof area on some of the buildings, but installation possibilities and costs were not analyzed further.

4.3.2 Case II: More DH import

For this case, the mass flow from the IHCS to the DHW heating substation was reduced to get a balanced BTES. This mass flow reduction led to an increased amount of DH import for DHW heating from 572 MWh, as shown in Table 5, to 1122 MWh. The mass flow was reduced by 55 % during cooling mode and by 100 % during heating mode. DHW heating was thus only covered by the IHCS during cooling mode, when excess heat was available. The simulated electricity use decreased from 1212 MWh, as shown in Table 5, to 1099 MWh for this case.

4.3.3 Long-term operation analysis

The COPs for the balanced cases and the unbalanced base case scenario for five-year operation are shown in Figure 11. The input data for the year 2015 was repeated for this analysis.
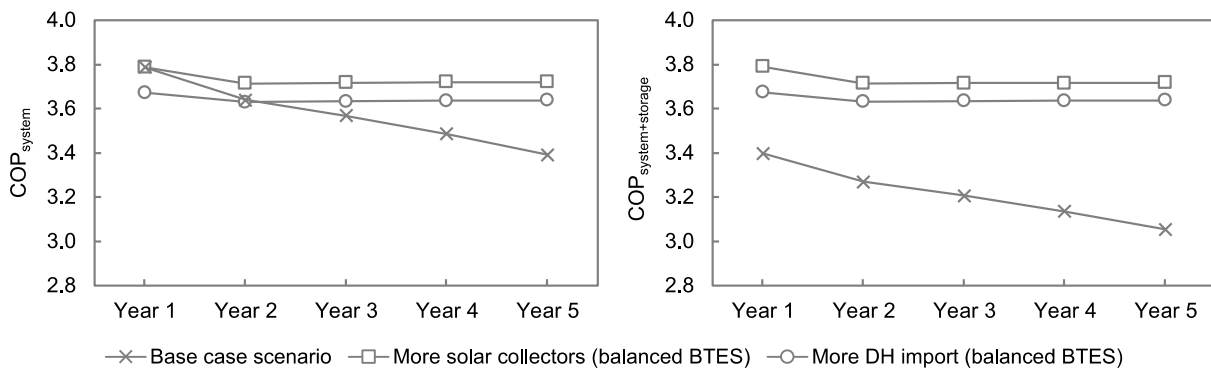

Figure 11. COPs for long-term operation.

The difference between the COPs in Figure 11 is that $COP_{system+storage}$ (right) included the annual heat balance of the BTES, see Equations 17 and 18. This balance was close to zero for the balanced cases, which is why their values for both COPs were nearly identical. The COPs decreased slightly from the first year to the second, most likely due to the initial temperature profile in the BTES, and remained constant afterwards. The COPs for the base case scenario decreased from year to year and thus showed continuous plant degradation. This degradation was mainly due to the decreasing average ground temperature, which led to higher pumping power for the BTES pump for heat extraction during heating mode as shown in Figure 12.
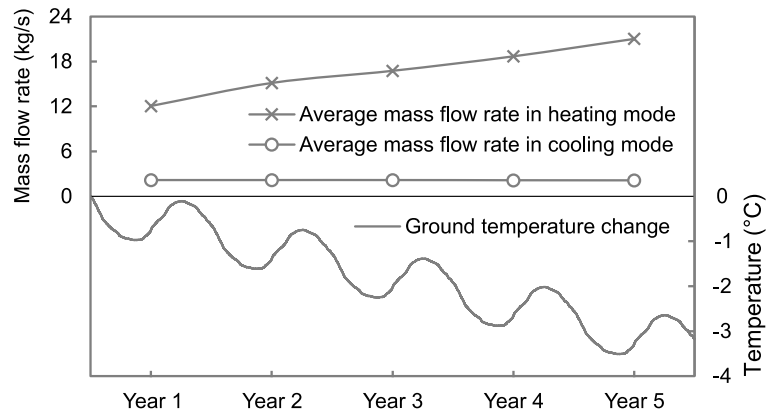
23

Figure 12. Long-term operation of BTES pump.

The BTES pump mass flow rate in cooling mode was much lower than in heating mode due to the larger temperature difference during heat injection. The long-term mass flow rate decrease during cooling mode was therefore insignificant.

5 Discussion

The aim of this study was a system level analysis of an existing IHCS with focus on the long-term thermal energy storage. Component models were therefore kept relatively simple and a validation on component level was out of scope. A flow coefficient was defined based on monthly electricity use, which led to a satisfactory correlation between simulated and measured system performance, see Figure 8 and Table 5. However, the electricity use of the IHCS was overestimated during a peak heating period in the beginning of the year. Since the heat pump models did not exceed the maximum power listed in the manufacturer specifications, this overestimation was most likely due to the calculated pumping power. The BTES pumps accounted for a large share of the pumping power, so a more detailed model of the BTES loop could improve the reliability of the results. However, this was impeded by lacking measurements and specifications.

The sensitivity analysis was performed by changing one parameter at a time. A change of 20 % was used for most parameters, but some exceptions were made. The efficiency of the heat pumps was varied within manufacturer specifications. For the supply and return temperatures, the temperature difference in the main heat exchanger was changed by 20 % for a fair comparison. However, the return temperatures from the buildings' heating and cooling systems, which were assumed constant in this study, can vary much more in reality and thus show more influence on the system performance than in the sensitivity analysis. A more detailed calculation of the return temperatures would therefore be desirable.

Changing the heat exchanger area did not influence the system performance significantly. An area reduction of 20 % reduced the COPs by less than 1 %, see Figure 10. This could either be due to

24

the lumping of the parallel heat exchangers in the system model, as explained in Section 3.1.6, or an oversized design. Most heat exchangers were dimensioned with an average temperature difference of 2°C, which led to relatively large heat exchanger areas. Confirming a possible oversizing by simulations with parallel units was outside the scope of this work.

Due to the cold climate in Norway, the building complex required more energy for heating than for cooling, see Figure 2. The insufficient charging of the BTES during summer led to a simulated annual BTES heat balance of -469 MWh, see Figure 9. Heat losses from components, pipes, and storages were neglected in this study. Including these losses would have led to a higher imbalance and thus to an even faster performance degradation than shown in Figure 11.

The solar collectors were a minor component of the IHCS due to the small number of installed collectors. They showed little effect on the system performance in the sensitivity analysis due to the low base value, see Figure 10. However, a significant increase in the number of collectors could lead to a balanced BTES and thus improve the long-term operation of the system, see Figure 11. The calculation of installation costs and an economic evaluation were outside the scope of this work.

Another possibility to avoid performance degradation was increased DH import. This case was analyzed and showed favorable long-term operation of the IHCS with the defined COPs due to reduced electricity use, see Figure 11. However, the increase in DH import exceeded the reduction in electricity use significantly and would thus most likely lead to increased operation costs. The calculation of operation costs with varying prices for electricity and DH was outside the scope of this work.

6   Conclusions

Dynamic simulations in Modelica were successfully applied to model an existing IHCS in Oslo, Norway. The simulation time for a one-year simulation was around 70 seconds despite the system's complexity. The short simulation time enables further analyses, e.g. parameter studies or dynamic optimization.

The system model was calibrated and a sensitivity analysis was performed. The results showed that the efficiency of the heat pumps and the annual heat balance of the BTES had strong influence on the system performance. The simulations showed a negative heat balance of the BTES (-469 MWh), which led to decreasing long-term performance. The $COP_{system+storage}$ was defined, which included this heat balance and thus gave a better indication of long-term performance even for a one-year simulation. This COP is therefore recommended to be used for one-year analyses of systems with long-term thermal storage.

Sustainable operation of the IHCS was possible by increasing the number of solar collectors from 140 to 830 or by importing more heat from the local DH system. However, the annual heat balance and system performance depended on the total heating and cooling demands, which may vary from year to year, as well as control setpoints, which were kept constant in this study. Future work could therefore include the analysis of more recent measurement data or improvement suggestions for the control strategy of the system. Model refinement, e.g. a more detailed calculation of the pumping power and/or the return temperatures from the building side, as well as an economic evaluation could also be included in future analyses.

Acknowledgements

References

1. European Union, *Directive 2010/31/EU of the European Parliament and of the Council of 19 May 2010 on the energy performance of buildings.* Official Journal of the European Union, 2010. **L 153**: p. 13–35.

2. International Energy Agency, *Heating and Cooling Technologies*, in *Transition to Sustainable Buildings: Strategies and Opportunities to 2050.* 2013, International Energy Agency.

3. Lund, H., et al., *4th Generation District Heating (4GDH): Integrating smart thermal grids into future sustainable energy systems.* Energy, 2014. **68**: p. 1-11. http://dx.doi.org/10.1016/j.energy.2014.02.089.

4. Jing, Z.X., et al., *Modelling and optimal operation of a small-scale integrated energy based district heating and cooling system.* Energy, 2014. **73**: p. 399-415. http://dx.doi.org/10.1016/j.energy.2014.06.030.

5. Marguerite, C., et al., *Simulation based multi-criteria evaluation of design scenarios for an industrial waste heat based micro district heating network supplying standard and low-energy buildings.* Energy Procedia, 2017. **116**: p. 128-137. http://dx.doi.org/10.1016/j.egypro.2017.05.061.

6. Zhu, N., et al., *Recent research and applications of ground source heat pump integrated with thermal energy storage systems: A review.* Applied Thermal Engineering, 2014. **71**(1): p. 142-151. http://dx.doi.org/10.1016/j.applthermaleng.2014.06.040.

7. Lanahan, M. and P. Tabares-Velasco, *Seasonal Thermal-Energy Storage: A Critical Review on BTES Systems, Modeling, and System Design for Higher System Efficiency.* Energies, 2017. **10**(6): p. 743. http://dx.doi.org/10.3390/en10060743.

8. You, T., et al., *A new solution for underground thermal imbalance of ground-coupled heat pump systems in cold regions: Heat compensation unit with thermosyphon.* Applied Thermal Engineering, 2014. **64**(1): p. 283-292. http://dx.doi.org/10.1016/j.applthermaleng.2013.12.010.

9.   Bayer, P., M. de Paly, and M. Beck, *Strategic optimization of borehole heat exchanger field for seasonal geothermal heating and cooling.* Applied Energy, 2014. **136**: p. 445-453. http://dx.doi.org/10.1016/j.apenergy.2014.09.029.

10.   Luo, J., et al., *Heating and cooling performance analysis of a ground source heat pump system in Southern Germany.* Geothermics, 2015. **53**: p. 57-66. http://dx.doi.org/10.1016/j.geothermics.2014.04.004.

11.   Capozza, A., A. Zarrella, and M. De Carli, *Long-term analysis of two GSHP systems using validated numerical models and proposals to optimize the operating parameters.* Energy and Buildings, 2015. **93**: p. 50-64. http://dx.doi.org/10.1016/j.enbuild.2015.02.005.

12.   Nam, Y., et al., *Study on the Performance of a Ground Source Heat Pump System Assisted by Solar Thermal Storage.* Energies, 2015. **8**(12): p. 12365. http://dx.doi.org/10.3390/en81212365.

13.   Han, Z., et al., *Numerical simulation of solar assisted ground-source heat pump heating system with latent heat energy storage in severely cold area.* Applied Thermal Engineering, 2008. **28**(11): p. 1427-1436. http://dx.doi.org/10.1016/j.applthermaleng.2007.09.013.

14.   Zhai, X.Q., et al., *A review for the applications and integrated approaches of ground-coupled heat pump systems.* Renewable and Sustainable Energy Reviews, 2011. **15**(6): p. 3133-3140. http://dx.doi.org/10.1016/j.rser.2011.04.024.

15.   Rad, F.M., A.S. Fung, and W.H. Leong, *Feasibility of combined solar thermal and ground source heat pump systems in cold climate, Canada.* Energy and Buildings, 2013. **61**: p. 224-232. http://dx.doi.org/10.1016/j.enbuild.2013.02.036.

16.   Arteconi, A., et al., *Experimental evaluation and dynamic simulation of a ground coupled heat pump for a commercial building.* International Journal of Energy Research, 2013. **37**(15): p. 1971-1980. http://dx.doi.org/10.1002/er.3059.

17.   Li, H., L. Sun, and Y. Zhang, *Performance investigation of a combined solar thermal heat pump heating system.* Applied Thermal Engineering, 2014. **71**(1): p. 460-468. http://dx.doi.org/10.1016/j.applthermaleng.2014.07.012.

18.   Carotenuto, A., R.D. Figaj, and L. Vanoli, *A novel solar-geothermal district heating, cooling and domestic hot water system: Dynamic simulation and energy-economic analysis.* Energy, 2017. **141**: p. 2652-2669. http://dx.doi.org/10.1016/j.energy.2017.08.084.

19.   Razavi, S.H., R. Ahmadi, and A. Zahedi, *Modeling, simulation and dynamic control of solar assisted ground source heat pump to provide heating load and DHW.* Applied Thermal Engineering, 2018. **129**: p. 127-144. http://dx.doi.org/10.1016/j.applthermaleng.2017.10.003.

20.   Sangi, R., et al., *Modeling and simulation of the heating circuit of a multi-functional building.* Energy and Buildings, 2016. **110**: p. 13-22. http://dx.doi.org/10.1016/j.enbuild.2015.10.027.

21.   Maccarini, A., et al., *Energy saving potential of a two-pipe system for simultaneous heating and cooling of office buildings.* Energy and Buildings, 2017. **134**: p. 234-247. http://dx.doi.org/10.1016/j.enbuild.2016.10.051.

22.   Wetter, M. and C. van Treeck, *IEA EBC Annex 60: New Generation Computing Tools for Building and Community Energy Systems*. 2017, International Energy Agency,.

23.	Liu, F., W. Zhu, and J. Zhao, *Model-based dynamic optimal control of a CO2 heat pump coupled with hot and cold thermal storages.* Applied Thermal Engineering, 2018. **128**: p. 1116-1125. http://dx.doi.org/10.1016/j.applthermaleng.2017.09.098.

24.	Wang, E., et al., *Performance prediction of a hybrid solar ground-source heat pump system.* Energy and Buildings, 2012. **47**: p. 600-611. http://dx.doi.org/10.1016/j.enbuild.2011.12.035.

25.	Rohde, D., et al. *Documentation of an Integrated Thermal Energy System for a Building Complex.* in *24th International Congress of Refrigeration.* 2015. Yokohama, Japan.

26.	Norwegian Institute of Bioeconomy Research. *Weather Data for Norway.* Accessed May 2017; Available from: http://lmt.bioforsk.no/agrometbase/getweatherdata_new.php.

27.	Modelica Association *Modelica® - A Unified Object-Oriented Language for Systems Modeling.* Language Specification, 2017. **Version 3.4**.

28.	Modelica Association. *Modelica Libraries.* Accessed March 2018; Available from: https://www.modelica.org/libraries.

29.	Bell, I.H., et al., *Pure and Pseudo-pure Fluid Thermophysical Property Evaluation and the Open-Source Thermophysical Property Library CoolProp.* Industrial & Engineering Chemistry Research, 2014. **53**(6): p. 2498-2508. http://dx.doi.org/10.1021/ie4033999.

30.	Incropera, F.P., et al., *Heat Exchangers*, in *Fundamentals of Heat and Mass Transfer.* 2007, John Wiley & Sons.

31.	Giraud, L., et al. *Presentation, Validation and Application of the DistrictHeating Modelica Library.* in *11th International Modelica Conference.* 2015. Versailles, France.

32.	Yang, J., A. Jacobi, and W. Liu, *Heat transfer correlations for single-phase flow in plate heat exchangers based on experimental data.* Applied Thermal Engineering, 2017. **113**: p. 1547-1557. http://dx.doi.org/10.1016/j.applthermaleng.2016.10.147.

33.	Sofrata, H., *Carnot and Lorenz cycles for dual absorption system.* Wärme - und Stoffübertragung, 1993. **28**(3): p. 107-116. http://dx.doi.org/10.1007/BF01541106.

34.	Østergaard, P.A. and A.N. Andersen, *Booster heat pumps and central heat pumps in district heating.* Applied Energy, 2016. **184**: p. 1374-1388. http://dx.doi.org/10.1016/j.apenergy.2016.02.144.

35.	Bauer, D., et al., *Thermal resistance and capacity models for borehole heat exchangers.* International Journal of Energy Research, 2011. **35**(4): p. 312-320. http://dx.doi.org/10.1002/er.1689.

36.	Spitler, J.D., R. Grundmann, and S. Javed. *Calculation Tool for Effective Borehole Thermal Resistance.* in *12th REHVA World Congress (CLIMA 2016).* 2016. Aalborg, Denmark.

37.	Spitler, J.D., S. Javed, and R.K. Ramstad, *Natural convection in groundwater-filled boreholes used as ground heat exchangers.* Applied Energy, 2016. **164**: p. 352-365. http://dx.doi.org/10.1016/j.apenergy.2015.11.041.

38.	Holmberg, H., et al., *Numerical model for non-grouted borehole heat exchangers, Part 2 - Evaluation.* Geothermics, 2016. **59**: p. 134-144. http://dx.doi.org/10.1016/j.geothermics.2014.11.002.

39.	Stephan, P., *Fundamentals of Heat Transfer*, in *VDI Heat Atlas.* 2010, Springer: Berlin Heidelberg. p. 15-30.

40.   Ramstad, R.K., et al., *Thermal conductivity map of the Oslo region based on thermal diffusivity measurements of rock core samples.* Bulletin of Engineering Geology and the Environment, 2015. **74**(4): p. 1275-1286. http://dx.doi.org/10.1007/s10064-014-0701-x.

41.   Sibbitt, B., et al., *The Performance of a High Solar Fraction Seasonal Storage District Heating System – Five Years of Operation.* Energy Procedia, 2012. **30**: p. 856-865. http://dx.doi.org/10.1016/j.egypro.2012.11.097.

42.   Partenay, V., et al., *The influence of the borehole short-time response on ground source heat pump system efficiency.* Energy and Buildings, 2011. **43**(6): p. 1280-1287. http://dx.doi.org/10.1016/j.enbuild.2011.01.009.

43.   Ruiz-Calvo, F., et al., *Experimental validation of a short-term Borehole-to-Ground (B2G) dynamic model.* Applied Energy, 2015. **140**: p. 210-223. http://dx.doi.org/10.1016/j.apenergy.2014.12.002.

44.   Xia, L., et al., *Experimental investigation and control optimization of a ground source heat pump system.* Applied Thermal Engineering, 2017. **127**: p. 70-80. http://dx.doi.org/10.1016/j.applthermaleng.2017.07.205.

45.   Beier, R.A., M.D. Smith, and J.D. Spitler, *Reference data sets for vertical borehole ground heat exchanger models and thermal response test analysis.* Geothermics, 2011. **40**(1): p. 79-85. http://dx.doi.org/10.1016/j.geothermics.2010.12.007.

46.   Herrero López, S., et al. *Dynamic Modelling of a Flat-Plate Solar Collector for Control Purposes*. in *11th International Modelica Conference*. 2015. Versailles, France.

47.   Dumont, O., et al. *Hot water tanks : How to select the optimal modelling approach?* in *12th REHVA World Congress (CLIMA 2016)*. 2016. Aalborg, Denmark.

48.   Mosallat, F., et al., *Modeling, Simulation and Control of Flat Panel Solar Collectors with Thermal Storage for Heating and Cooling Applications.* Procedia Computer Science, 2013. **19**: p. 686-693. http://dx.doi.org/10.1016/j.procs.2013.06.091.

49.   ASHRAE, *Geothermal Energy*, in *ASHRAE Handbook - Heating, Ventilating, and Air-Conditioning Applications (SI Edition)*. 2015, American Society of Heating, Refrigerating and Air-Conditioning Engineers, Inc.